Inorg. Chem. **2003**, *42*, 1499−1507

Crystal and Molecular Structures of Alkali Oxalates: First Proof of a Staggered Oxalate Anion in the Solid State

Robert E. Dinnebier,* Sascha Vensky, Martin Panthöfer, and Martin Jansen*

Max Planck Institute for Solid State Research, Heisenbergstrasse 1, D-70569 Stuttgart, Germany

Received September 12, 2002

The molecular and crystal structures of solvent-free potassium, rubidium, and cesium oxalates have been determined ab initio from high-resolution synchrotron and X-ray laboratory powder patterns. In the case of potassium oxalate $K_2C_2O_4$ ($a = 10.91176(7)$ Å, $b = 6.11592(4)$ Å, $c = 3.44003(2)$ Å, orthorhombic, *Pbam*, $Z = 2$), the oxalate anion is planar, whereas in cesium oxalate $Cs_2C_2O_4$ ($a = 6.62146(5)$ Å, $b = 11.00379(9)$ Å, $c = 8.61253(7)$ Å, $\beta = 97.1388(4)°$, monoclinic, $P2_1/c$, $Z = 4$) it exhibits a staggered conformation. For rubidium oxalate at room temperature, two polymorphs exist, one (β-$Rb_2C_2O_4$) isotypic to potassium oxalate ($a = 11.28797(7)$ Å, $b = 6.29475(4)$ Å, $c = 3.62210(2)$ Å, orthorhombic, *Pbam*, $Z = 2$) and the other (α-$Rb_2C_2O_4$) isotypic to cesium oxalate ($a = 6.3276(1)$ Å, $b = 10.4548(2)$ Å, $c = 8.2174(2)$ Å, $\beta = 98.016(1)°$, monoclinic, $P2_1/c$, $Z = 4$). The potassium oxalate structure can be deduced from the AlB_2 type, and the cesium oxalate structure from the $Hg_{99}As$ type, respectively. The relation between the two types of crystal structures and the reason for the different conformations of the oxalate anion are discussed.

Introduction

Alkali oxalates play an important role in nature and chemistry. The sodium and potassium salts of oxalic acid are found in many plants (clover, sorrel, salicornia, spinach, rhubarb, bamboo shoots, cacao, roots, and tree barks). Oxalates find some technical and medical applications such as stain removal in photography, metal coatings for stainless steel, nickel, chromium, titanium, and their alloys, cleaning and bleaching of natural fibers, textile dyeing, anticoagulants in medical tests, and dental seals. Furthermore potassium and sodium oxalate complexes are able to pass the gastric mucous membrane, and therefore they are the main components of kidney stones.

Nevertheless, the long-standing efforts aimed at understanding the characteristic structural features of the oxalate anion using conventional concepts of chemical bonding still remain without closure. In the first place, the C−C bond lengths of oxalate anions (1.567(2) Å)[1] are about 0.04 Å too large for two sp^2-hybridized C atoms (1.515 Å).[2−4] This well-established experimental fact is indicative of a bond order of 1 or even less. Thus, one would expect a staggered conformation (point symmetry D_{2d}) of the oxalate anions to be preferred. This view is strongly supported by quantum mechanical calculations.[5] However, experimentally the opposite is found: only few exceptions from planarity (D_{2h}) have been reported so far. If crystal structures with *R* values >14% are disregarded, only $NaHC_2O_4 \cdot H_2O$ (twist angle of 13°),[6] KHC_2O_4 (13°),[7−9] $(NH_4)_2C_2O_4 \cdot H_2O$ (27°),[10−12] $(NH_4)_2C_2O_4 \cdot H_2O_2$ (28°),[13] and $BaC_2O_4 \cdot 0.5H_2O$ (30°)[14] remain to be considered. Evidently, in each of these instances the oxalate is involved in significant bonding interactions, i.e.,

* Authors to whom correspondence should be addressed. E-mail: r.dinnebier@fkf.mpg.de (R.E.D.); m.jansen@fkf.mpg.de (M.J.). Fax: (+49) 711-689-1502.

(1) Küppers, H. *Acta Crystallogr., Sect. B: Struct. Sci.* **1973**, *29*, 318−327.
(2) Bastiansen, O.; Trætteberg, M. *Tetrahedron* **1962**, *17*, 147−154.
(3) Beagley, B.; Small, R. W. H. *Proc. R. Soc. A* **1963**, *276*, 469−491.
(4) Coulson, C. A.; Skancke, P. N. *J. Chem. Soc.* **1962**, 2775−2782.
(5) Colby College, Chemistry Department, Paul J. Schupf Computational Chemistry Lab, Waterville, USA; http://www.colby.edu/chemistry/webmo/mointro.html.
(6) Tellgren, R.; Olovsson, I. *J. Chem. Phys.* **1971**, *54*, 127−134.
(7) Pedersen, B. F. *Acta Chem. Scand.* **1968**, *22*, 2953−2964.
(8) Einspahr, H.; Marsh, R. E.; Donohue, J. *Acta Crystallogr., Sect. B: Struct. Sci.* **1972**, *28*, 2194−2198.
(9) Kholodkovskaya, L. N.; Trunov, V. K.; Tskhelashvili, N. B. *J. Struct. Chem.* **1990**, *31*, 509−511.
(10) Robertson, J. H. *Acta Crystallogr.* **1965**, *18*, 410−417.
(11) Padmanabhan, V. M.; Srikantha, S.; Medhi Ali, S. *Acta Crystallogr.* **1965**, *18*, 567−568.
(12) Taylor, J. C.; Sabine, T. M. *Acta Crystallogr., Sect. B: Struct. Sci.* **1972**, *28*, 3340−3351.
(13) Pedersen, B. F. *Acta Crystallogr., Sect. B: Struct. Sci.* **1972**, *28*, 746−754.
(14) Mutin, J. C.; Dusausoy, Y.; Protas, J. *J. Solid State Chem.* **1981**, *36*, 356−364.

10.1021/ic0205536 CCC: $25.00
Published on Web 02/06/2003

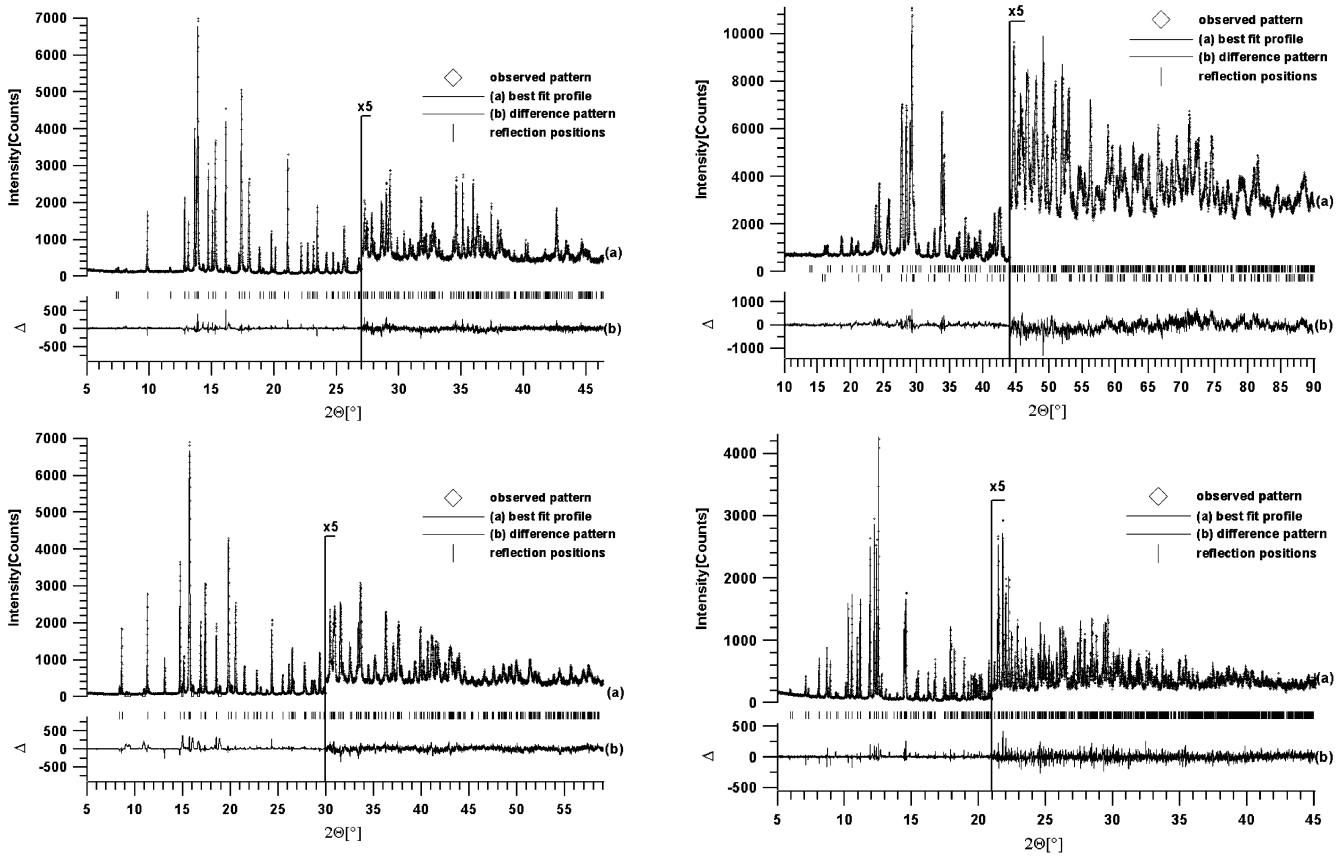

Figure 1. Scattered X-ray intensities for $A_2C_2O_4$ [A = K (top left), β-Rb (bottom left), α-Rb (top right), and Cs (bottom right)] at ambient conditions as a function of diffraction angle 2Θ. Shown are the observed patterns (diamonds), the best Rietveld-fit profiles (line) and the enlarged difference curves between observed and calculated profiles (below in an additional window). The high-angle parts are enlarged by a factor of 5, starting at 2Θ values of 27° ($K_2C_2O_4$), 30° (β-$Rb_2C_2O_4$), 44° (α-$Rb_2C_2O_4$), and 21° ($Cs_2C_2O_4$). The wavelengths were $\lambda = 0.7$ Å for $K_2C_2O_4$ and $Cs_2C_2O_4$, 0.83 Å for β-$Rb_2C_2O_4$, and 1.54 Å for α-$Rb_2C_2O_4$. In case of β-$Rb_2C_2O_4$, several excluded regions in the powder pattern have been defined, in order to account for small amounts of $Rb_2C_2O_4 \cdot H_2O$ present in the sample, and in the case of α-$Rb_2C_2O_4$, β-$Rb_2C_2O_4$ was included as a second phase.

H-bonds. This raises the question, whether the strong prevalence of the planar configuration is related to intermolecular interactions rather than to the intramolecular electron density distribution. In order to empirically clarify this issue, we have undertaken a systematic structural investigation of ionic oxalates that exhibit the lowest possible covalent bonding to the cations, i.e., the anhydrous oxalates of potassium, rubidium, and cesium.

Due to the hygroscopic nature of the oxalates, only few instances of successful single-crystal syntheses of solvent-free oxalates in sufficient size and quality for single-crystal analysis have been reported so far: by diffusion ($Ag_2C_2O_4$),[15] slow evaporation from an aqueous solution ($Li_2C_2O_4$,[16] $Na_2C_2O_4$,[17] $K_2Be(C_2O_4)_2$[18]), or hydrothermal crystallization (SrC_2O_4).[19]

Therefore we performed high-resolution X-ray powder diffraction experiments to determine the crystal structures of $K_2C_2O_4$ (**I**), α-$Rb_2C_2O_4$ (**II**-α), β-$Rb_2C_2O_4$ (**II**-β), and $Cs_2C_2O_4$ (**III**) at ambient conditions.

Experimental Section

Potassium, rubidium, and cesium oxalate were prepared by dehydration of the corresponding monohydrates for 18 h at 373 K in a vacuum. Potassium oxalate monohydrate was used as purchased ($K_2C_2O_4 \cdot H_2O$, Fluka, puriss. p.a.). Rubidium and cesium oxalate monohydrate were synthesized by reaction of the corresponding carbonates (Rb_2CO_3, Alfa Aesar, p.a.; Cs_2CO_3, Chempur, p.a.) and oxalic acid dihydrate ($H_2C_2O_4 \cdot 2H_2O$, Fluka, puriss. p.a.) in an aqueous solution. The solution was stirred for 12 h at 353 K, and the water was subsequently removed by distillation. The precipitates were washed with diethyl ether and acetone. The dehydrated oxalates were handled under argon as an inert atmosphere to prevent a possible contamination by water.

X-ray powder diffraction data of the room temperature phases of **I**, **II**-β, and **III** were collected at $T = 295$ K on beamline X3B1 of the Brookhaven National Synchrotron Light Source in transmission geometry with the samples sealed in 0.7 mm (**I**), 0.5 mm (**II**-β), and 0.3 mm (**III**) lithiumborate glass (Hilgenberg glass No. 50) capillaries (Figure 1). X-rays of wavelength 0.7 Å (**I** and **III**) and 0.83 Å (**II**-β) were selected by a double Si(111) monochromator. Wavelengths and the zero point were determined from eight well-defined reflections of the NBS1976 flat plate alumina standard. The diffracted beam was analyzed with a Ge(111) crystal and detected with a Na(Tl)I scintillation counter employing a pulse

(15) Naumov, D. Y.; Virovets, A. V.; Podberezskaya, N. V.; Boldyreva, E. V. *Acta Crystallogr., Sect C: Cryst. Struct. Commun.* **1995**, *51*, 60−62.
(16) Beagley, B.; Small, R. W. H. *Acta Crystallogr.* **1964**, *17*, 783−788.
(17) Reed, D. A.; Olmstead, M. M. *Acta Crystallogr., Sect. B: Struct. Sci.* **1981**, *37*, 938−939.
(18) Jaber, P. M.; Faure, R.; Loiseleur, H. *Acta Crystallogr., Sect. B: Struct. Sci.* **1978**, *34*, 429−431.
(19) Price, D. J.; Powell, A. K.; Wood, P. T. *Polyhedron* **1999**, *18*, 2499−2503.

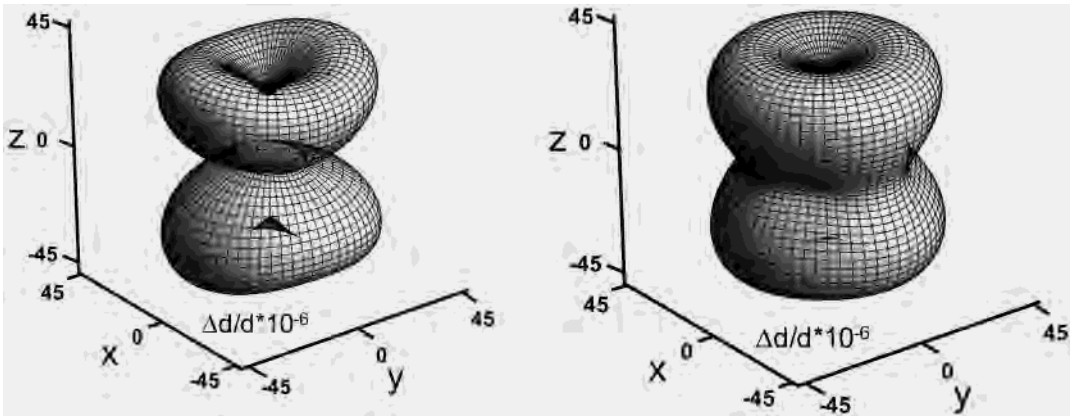

Figure 2. Three-dimensional semitransparent representation of the microstrain distribution of $K_2C_2O_4$ (left), and β-$Rb_2C_2O_4$ (right) at ambient conditions. The scale is in $\Delta d/d \times 10^{-6}$ strain.

Table 1. Crystallographic Data for $A_2C_2O_4$ [A = K, Rb, Cs]

	$K_2C_2O_4$	β-$Rb_2C_2O_4$	α-$Rb_2C_2O_4$	$Cs_2C_2O_4$
formula	$K_2C_2O_4$	$Rb_2C_2O_4$	$Rb_2C_2O_4$	$Cs_2C_2O_4$
temp (K)	295	295	260	295
fw (g/mol)	166.216	258.955	258.955	353.830
space group	*Pbam*	*Pbam*	$P2_1/c$	$P2_1/c$
Z	2	2	4	4
a (Å)	10.91176(7)	11.28797(7)	6.3276(1)	6.62146(5)
b (Å)	6.11592(4)	6.29475(4)	10.4548(2)	11.00379(9)
c (Å)	3.44003(2)	3.62210(2)	8.2174(2)	8.61253(7)
α (deg)	90	90	90	90
β (deg)	90	90	98.016(1)	97.1388(4)
γ (deg)	90	90	90	90
V (Å^3)	229.572(3)	257.369(3)	538.30(2)	622.654(9)
ρ_{calc} (g/cm^3)	2.404	3.341	3.195	3.774
ρ_{obsd} (g/cm^3)	2.409(1)		3.172(2)	3.792(4)
wavelength (Å)	0.70003(5)	0.82978(4)	1.54060	0.70003(5)
capillary diam (mm)	0.7	0.5	0.2	0.3
R-p (%)[a]	4.9	5.1	4.4	7.1
R-wp (%)[a]	5.9	6.1	5.8	8.3
R-F^2 (%)[a]	6.4	8.7	8.9	8.2

[a] R-p, R-wp, and R-F^2 as defined in GSAS:[25] R-p $= \sum_i|y_i(\text{obsd}) - y_i(\text{calcd})|/[\sum_i y_i(\text{obsd})]$. R-wp $= \{\sum_i w_i(y_i(\text{obsd}) - y_i(\text{calcd}))^2/[\sum_i w_i(y_i(\text{obsd}))^2]\}^{1/2}$. R-F^2 $= \sum_i|F_i(\text{obsd})^2 - F_i(\text{calcd})^2|/[\sum_i|F_i(\text{obsd})^2|]$.

height discriminator in the counting chain. The incoming beam was monitored by an ion chamber for normalization purposes in order to take the decay of the primary beam into account. In this parallel beam configuration, the resolution is determined by the analyzer crystal instead of slits.[20] Data were taken in 2Θ steps of 0.005° from 5° to 46.34° for 7.2 h (**I**), from 5° to 59.06° for 9.3 h (**II**-β), and from 3° to 45.14° for 9.4 h (**III**) (see Table 1). Although Θ-scans did not show serious crystallite size effects, the samples were spun during measurement for better particle statistics. The powder patterns of (I) and (III) exhibit several peaks of very small amounts (<0.5%) of the corresponding monohydrate phases.

X-ray powder diffraction data of the α-phase of rubidium oxalate (**II**-α) were collected at room temperature with a Stoe Stadi-P transmission diffractometer (primary beam Johann-type Ge monochromator for Cu Kα_1 radiation, linear PSD) in 2Θ steps of 0.01° from 10° to 90° at a temperature of $T = 260$ K for 67 h with the sample sealed in a glass capillary of 0.2 mm diameter (Hilgenberg, glass No. 50) (Figure 1). Weak reflections corresponding to small traces of the β-phase as an additional phase were observed in the scan. Further experimental details are given in Table 1.

Data reduction on all four data sets was performed using the GUFI program.[21] Indexing with ITO[22] led to similar primitive orthorhombic unit cells for **I** and **II**-β and to primitive monoclinic unit cells for **II**-α and **III** with lattice parameters given in Table 1. The number of formula units per unit cell could be determined to be $Z = 2$ for **I** and **II**-β and $Z = 4$ for **II**-α and **III**, respectively, from packing considerations and density measurements. The extinctions found in the powder patterns indicated either *Pbam* or *Pba*2 for **I** and **II**-β and $P2_1/c$ for **II**-α and **III**, respectively, as the most probable space groups. *Pbam* and $P2_1/c$ could later be confirmed by Rietveld refinements[23] to be the appropiate groups. The peak profiles and precise lattice parameters were determined by LeBail-type fits[24] using the programs GSAS[25] and FULLPROF.[26,27] The background was modeled manually using GUFI. The peak profile was described by a pseudo-Voigt function in combination with a special function that accounts for the asymmetry due to axial divergence.[28,29] The powder pattern of **I** and **II**-β exhibit severe anisotropic peak broadening caused by lattice strain, with the sharpest peaks along the [001] direction having a 2Θ full width at half-maximum (fwhm) of 0.014° for **I** and 0.021° for **II**-β, respectively. The phenomenological strain model of Stephens[30] as implemented in GSAS was used to model the anisotropy of the fwhm. Four parameters were refined for the orthorhombic phases. A three-dimensional representation of the isosurface of the microstrain is shown in Figure 2.

The crystal structures of **I** and **III** were solved in the following way with use of the DASH structure solution package[31] for the NSLS synchrotron and laboratory data sets: The measured powder patterns were subjected to a Pawley refinement[32] in space groups *Pbam* for **I** and $P2_1/c$ for **III** in order to extract correlated integrated intensities from the pattern. Good fits to the data were obtained.

(20) Cox, D. E. *Handbook of Synchrotron Radiation, Vol.* 3, *Chapter 5 Powder Diffraction*; Brown, G., Moncton, D. E., Eds.; Elsevier: Amsterdam, 1991.
(21) Dinnebier, R. E.; Finger, L. *Z. Kristallogr.* **1998**, *Suppl. Issue 15*, 148.
(22) Visser, J. W. *J. Appl. Crystallogr.* **1969**, *2*, 89−95.
(23) Rietveld, H. M. *J. Appl. Crystallogr.* **1969**, *2*, 65−71.
(24) Le Bail, A.; Duroy, H.; Fourquet, J. L. *Mater. Res. Bull.* **1988**, *23*, 447−452.
(25) Larson, A. C.; von Dreele, R. B. *GSAS*, version 2002; Los Alamos National Laboratory Report LAUR 86-748; Los Alamos National Laboratory: Los Alamos, NM, 1994.
(26) Rodriguez-Carvajal, J. *Abstracts of the Satellite Meeting on Powder Diffraction of the XV Congress of the IUCr*; p 127; Toulouse, France, 1990.
(27) Rodriguez-Carvajal, J. *Fullproof.2k*, version 1.9c; Laboratoire Leon Brillouin: Gif-sur-Yvette, France, 2001.
(28) Thompson, P.; Cox, D. E.; Hastings, J. B. *J. Appl. Crystallogr.* **1987**, *20*, 79−83.
(29) Finger, L. W.; Cox, D. E.; Jephcoat, A. P. *J. Appl. Crystallogr.* **1994**, *27*, 892−900.
(30) Stephens, P. W. *J. Appl. Crystallogr.* **1999**, *32*, 281−289.
(31) David, W. I. F.; Shankland, K.; Shankland, N. *Chem. Commun.* **1998**, 931−932.
(32) Pawley, G. S. *J. Appl. Crystallogr.* **1981**, *14*, 357−361.

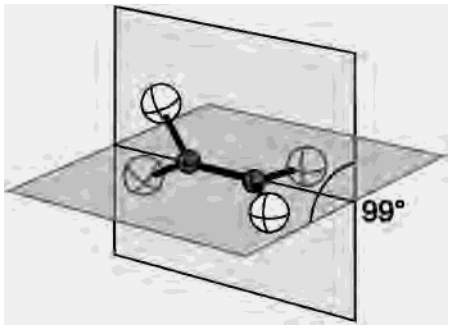

Figure 3. Sketch of the oxalate anion as found in $Cs_2C_2O_4$.

An internal coordinate description of the oxalate moiety (Figure 3) was constructed using bond lengths, angles, and torsion angles from corresponding hydrated phases $K_2C_2O_4 \cdot H_2O$,[33−36] and $Cs_2C_2O_4 \cdot 2H_2O$.[37] The torsion angles between the two carboxyl groups could not be assigned precise values in advance, and thus they were treated as variables for refinement in the simulated annealing procedure. The positions of the crystallographically independent alkali cations (one in the case of **I** and **II**-β; two in the case of **II**-α and **III**) as well as the position, orientation, and conformation of the oxalate anions in the unit cell were postulated, and the level of agreement between the trial structure and the experimental diffraction data was quantified by

$$\chi^2 = \sum_h \sum_k [(I_h - c|F_h|^2)(V^{-1})_{hk}(I_k - c|F_k|^2)]$$

Here I_h and I_k are Lorentz−polarization corrected, extracted integrated intensities from the Pawley refinement of the diffraction data, V_{hk} is the covariance matrix from the Pawley refinement, c is a scale factor, and $|F_h|$ and $|F_k|$ are the structure factor magnitudes calculated from the trial structure. The trial structure was subjected to a global optimization[31] where the torsion angle between the carboxyl groups and the bond length between the carbon atoms were the only internal degrees of freedom. The external degrees of freedom consisted of the fractional coordinates describing the positions of the alkali cations and the oxalate anions, and four quaternions[38] describing the orientation of the molecule. The structure giving the best fit to the data was validated by Rietveld refinement of the fractional coordinates obtained at the end of the simulated annealing run.

Rietveld refinements were performed on all powder patterns of **I**, **II**-β, **II**-α, and **III** using the program package GSAS (Figure 1). The background was modeled manually using GUFI. No additional phases were included in the refinement of **I**, **II**-β, and **III**, but in the case of **II**-β, several excluded regions containing reflections of rubidium oxalate hydrate were defined. In the refinement of **II**-α, the polymorph **II**-β was included as an additional phase (about 18 wt %). The peak profile was described by a pseudo-Voigt function, in combination with a special function that accounted for the asymmetry due to axial divergence.[28,29] Due to the excellent reflection-to-parameter ratio, no soft constraints were necessary to stabilize the refinements. Agreement factors (R values) are listed in Table 1, the coordinates are given in Table 2, and a selection of intra- and intermolecular distances and angles is given in Table 3.

Table 2. Positional Parameters and Temperature Factors for $A_2C_2O_4$ [A = K, Rb, Cs] at Ambient Conditions

atom	x	y	z	U_i/U_e (Å^2)
		$K_2C_2O_4$		
K(1)	0.34860(6)	0.59497(9)	$^1/_2$	0.0214(2)
C(1)	0.4383(2)	1.0699(4)	0	0.0195(7)
O(1)	0.4505(1)	1.2729(3)	0	0.0268(6)
O(2)	0.3408(2)	0.9639(2)	0	0.0190(5)
		β-$Rb_2C_2O_4$		
Rb(1)	0.34720(5)	0.59308(8)	$^1/_2$	0.0283(2)
C(1)	0.4402(3)	1.0632(6)	0	0.00(1)[a]
O(1)	0.4517(2)	1.2584(4)	0	0.0006(8)
O(2)	0.3486(2)	0.9706(3)	0	0.00(1)[a]
		α-$Rb_2C_2O_4$		
Rb(1)	0.2827(2)	0.2938(1)	0.9790(2)	0.0533(5)
Rb(2)	0.2306(2)	0.5851(1)	0.3350(2)	0.0484(5)
C(1)	0.6904(6)	0.0459(5)	0.7802(7)	0.056(1)
C(2)	0.8215(6)	0.1035(3)	0.6544(7)	0.056(1)
O(1)	0.5518(9)	0.1255(6)	0.8050(8)	0.056(1)
O(2)	0.7124(2)	−0.0583(5)	0.8369(8)	0.056(1)
O(3)	0.7949(7)	0.1047(5)	0.5090(8)	0.056(1)
O(4)	0.9909(8)	0.1570(5)	0.7155(8)	0.056(1)
		$Cs_2C_2O_4$		
Cs(1)	0.2840(2)	0.2948(1)	0.9827(2)	0.0307(5)
Cs(2)	0.2294(2)	0.5886(1)	0.3316(2)	0.0322(5)
C(1)	0.691(1)	0.0560(6)	0.7777(7)	0.034(2)
C(2)	0.833(1)	0.1115(4)	0.6652(9)	0.034(2)
O(1)	0.547(1)	0.1256(9)	0.8075(8)	0.034(2)
O(2)	0.724(2)	−0.0511(6)	0.8309(8)	0.034(2)
O(3)	0.778(1)	0.1108(6)	0.5180(9)	0.034(2)
O(4)	1.001(1)	0.1541(7)	0.733(1)	0.034(2)

[a] Absorption correction was only applied to the data set measured at λ = 1.54 Å, but not for data sets measured at higher energies, explaining the low-temperature factor for oxygen in the case of the refinement of β-$Rb_2C_2O_4$.

Table 3. Selected Bond Lengths (Å) and Angles (deg) for $A_2C_2O_4$ [A = K, Rb, Cs] at Ambient Conditions[a]

	$K_2C_2O_4$	β-$Rb_2C_2O_4$	α-$Rb_2C_2O_4$	$Cs_2C_2O_4$
distances (Å)				
C−C	1.595(3)	1.567(5)	1.536(7)	1.56(1)
C−O	1.246(3) 1.249(3)	1.187(4) 1.236(5)	1.19(1)− 1.25(1)	1.27(1)− 1.28(1)
A(1)−O	2.806(2)− 2.901(1)	2.960(2)− 3.051(2)	2.888(6)− 3.386(5)	3.069(9)− 3.557(9)
A(2)−O			2.816(7)− 3.580(7)	3.015(8)− 3.737(9)
angles (deg)				
O−C−O	127.5(2)	125.4(3)	113.2(5) 126.6(5)	125.7(8) 125.8(8)
torsion angles (deg)				
O−C−C−O	0.0(3)	0.0(4)	94(3)	99(1)

[a] The given esd's are Rietveld statistical estimates and should be multiplied by a factor of up to 6 according to ref 52.

Guinier−Simon measurements (Enraf-Nonius FR 553, Cu Kα_1, Johansson monochromator) were conducted from room temperature up to 373 K. Densities of the alkali oxalates were determined by use of a He pycnometer (Micromeritics AccuPyc 1330 GB). IR data were recorded using the KBr disk method (1 mg of oxalates at 500 mg of KBr, prepared in a glovebox in an argon atmosphere) using a Bruker IFS 113v (Karlsruhe) FTIR spectrometer. Raman spectra were recorded of samples in sealed quartz capillaries (diameter 1 mm) using a Jobin Yvon (Horiba) Raman spectrometer.

Results and Discussion

Freshly prepared anhydrous rubidium oxalate consists of a mixture of both phases of rubidium oxalate with the

(33) Pedersen, B. F. *Acta Chem. Scand.* **1964**, *18*, 1635−1641.
(34) Hodgson, D. J.; Ibers, J. A. *Acta Crystallogr., Sect. B: Struct. Sci.* **1969**, *25*, 469−477.
(35) Sequeira, A.; Srikanta S.; Chidambaram, R. *Acta Crystallogr., Sect. B: Struct. Sci.* **1970**, *26*, 77−80.
(36) Jovanovski, G.; Thomas, J. O.; Olovsson, I. *Acta Crystallogr., Sect. B: Struct. Sci.* **1987**, *43*, 85−92.
(37) Kholodkovskaya, L. N.; Trunov, V. K.; Tskhelashvili, N. B. *J. Struct. Chem.* **1990**, *31*, 667−670.
(38) Leach, A. R. *Molecular Modelling Principles and Applications*; Addison-Wesley Longman Ltd.: Reading, MA, 1996; pp 2−4.

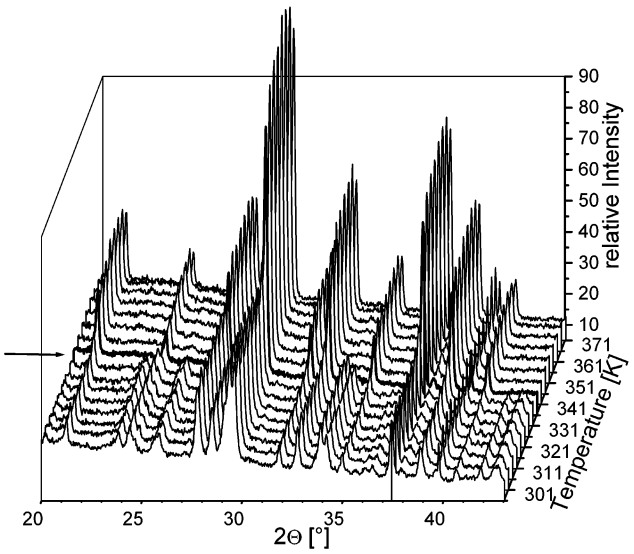

Figure 4. Guinier−Simon image plate recordings of $Rb_2C_2O_4$ as a function of temperature in the range 300.5−370.5 K. Whereas at room temperature the α-and *β*-phases coexist, the α-phase disappears completely at 333(2) K.

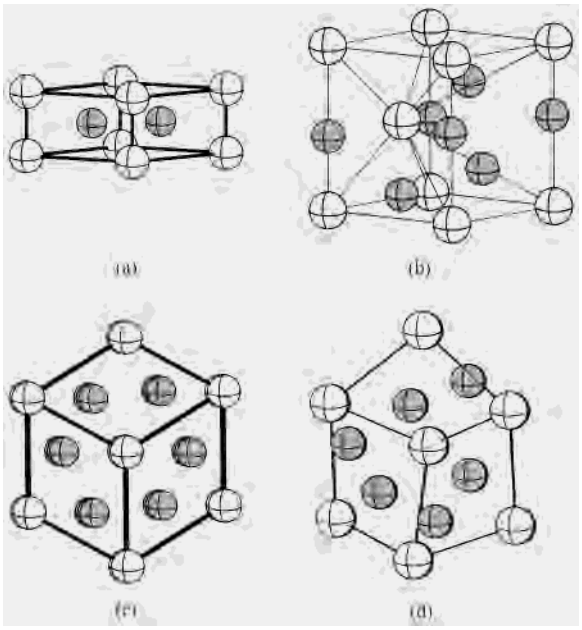

Figure 5. Packing types of $K_2C_2O_4$ (AlB_2-type) (a, c) and $Cs_2C_2O_4$ ($Hg_{99}As_1$-type) (b, d). The relation between the two structure types is visible in projections c and d. Alkali metal positions are in light gray, and the positions of the centers of mass of the oxalate anions are in white.

α-phase (**II**-α) as the predominating phase. Heating the α-phase above room temperature or storing at room temperature for some time leads to a complete transition into *β*-rubidium oxalate (**II**-*β*) (Figure 4).

The crystal structures of **I** and **II**-*β* are isotypic. They can be viewed as distorted AlB_2-type layer structures (3% distortion from hexagonal metric). The center of gravity of the oxalate anion is in the origin of a hexagonal unit cell, and two alkali cations are located close to $^1/_3{}^2/_3{}^1/_2$ and $^2/_3{}^1/_3{}^1/_2$ (Figure 5), thus forming alternating layers of oxalate anions and alkali cations. The planar oxalate anions are located on a mirror plane, forming infinite parallel chains along the *c*-direction with the length of the *c*-axis as the spacer. Each oxygen atom of the oxalate anions is coordinated to four alkali cations. Pairs of potassium cations (distance 3.502(1) Å; rubidium cations 3.643(1) Å; Table 3), which are interconnected by parallel (C−C bond) oxalates in a zigzag manner, form infinite parallel double chains along the *c*-axis. In the *a*-direction, the double chains are alternately inclined by approximately ±20° against the *a*-axis, leading to a herringbone arrangement (Figure 6). Each alkali cation is surrounded by eight oxygen atoms in the form of a distorted cube (Figure 7). Two cubes form a pair via a common face, and these pairs are stacked to infinite chains along the *c*-axis via common faces. Therefore, each cube shares three faces with neighboring cubes. Four of the side edges of a double cube are shared with four neighboring double cubes. Each oxalate chain is connected to four double chains of alkali cations and vice versa.

In contrast to the crystal structures of **I** and **II**-*β*, the isotypic crystal structures of **II**-α and **III** are not layer but framework structures (Figure 6). Each of the two crystallographically different alkali cations is surrounded by a different number of oxygen atoms forming irregular polyhedra (Figure 7). The alkali atoms Cs(1) and Rb(1), respectively, are coordinated to nine oxygen atoms (distances 3.069(9)−3.557(9) Å for cesium; 2.888(6)−3.386(5) Å for rubidium; Table 3) which belong to six different oxalate anions in the form of a distorted tetragonal antiprism capped at one of its trigonal planes. Consequently, two of the oxalate anions are side-on coordinated to the alkali cation, while one is end-on coordinated. Each alkali cation Cs(1)/Rb(1) is surrounded by eight alkali cations (six Cs(2)/Rb(2) and two Cs(1)/Rb(1)) in the second neighbor shell. Two alkali cations are located on top of the tetragonal planes, while each of the remaining six atoms is located on top of a trigonal face. The trigonal faces, built by the two side-on coordinated oxalate anions, are not capped. The alkali cations Cs(2)/Rb(2) are coordinated to 10 oxygen atoms (distances 3.015(8)−3.737(9) Å for cesium; distances 2.816(7)−3.580(7) Å for rubidium; Table 3) belonging to only five different oxalate anions in the form of an irregular polyhedron. This can best be described as a distorted trigonal prism with twisted roof and two additional oxygen atoms capping each of the tetragonal side faces of the prism. The roof is twisted by approximately 45°. Two end-on coordinated oxalate anions form the tetragonal base plane of the prism. Two oxygen atoms of two different oxalate anions form the roof. One of these oxalates is coordinated with only one oxygen atom therefore having the shortest alkali oxygen distance of 3.015(8) Å for cesium, and 2.816(7) Å for rubidium, respectively, while the other anion is coordinated with three oxygen atoms building one of the two caps. The other cap is formed by a side-on coordinated oxalate anion. Each alkali cation Cs(2)/Rb(2) is surrounded by eight alkali cations (six Cs(1)/Rb(1) and two Cs(2)/Rb(2)) in the second neighbor shell.

The positions of the centers of gravity of the oxalate anions form a *hcp*-type structure (maximum deviation of 3% and 0.8° from hexagonal metric, respectively) with the (idealized) positions of the oxalate anions at 000, $^1/_3{}^2/_3{}^1/_2$ and the alkali

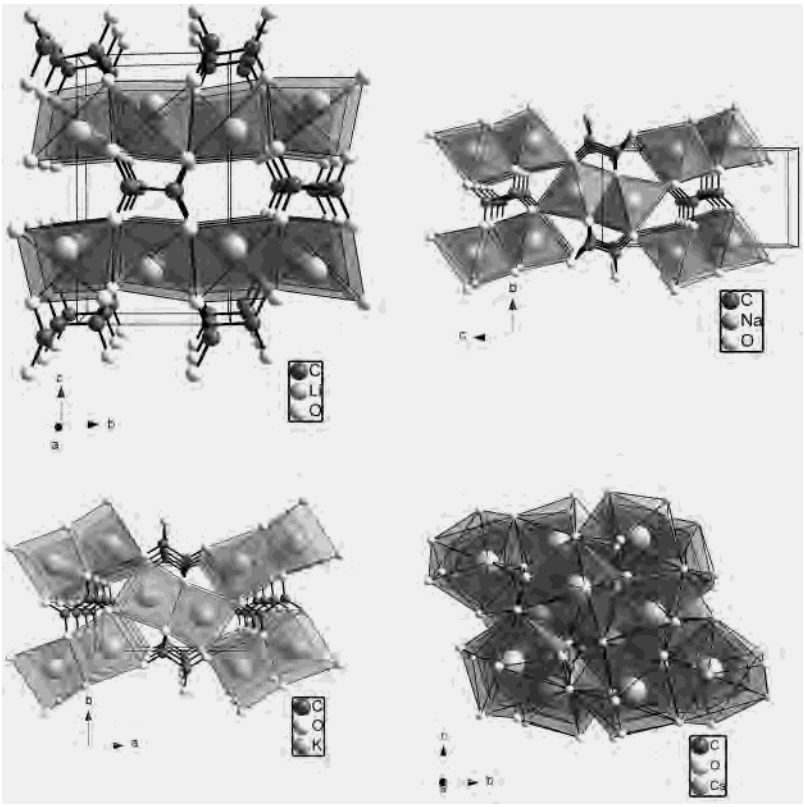

Figure 6. Crystal structures of $A_2C_2O_4$ [A = Li (top left),[16] Na (top right),[17] K, β-Rb (bottom left), α-Rb, Cs (bottom right)] in different projections. Oxygen positions are in white, carbon positions are in dark gray, and alkali metal positions and their corresponding polyhedra are in light gray.

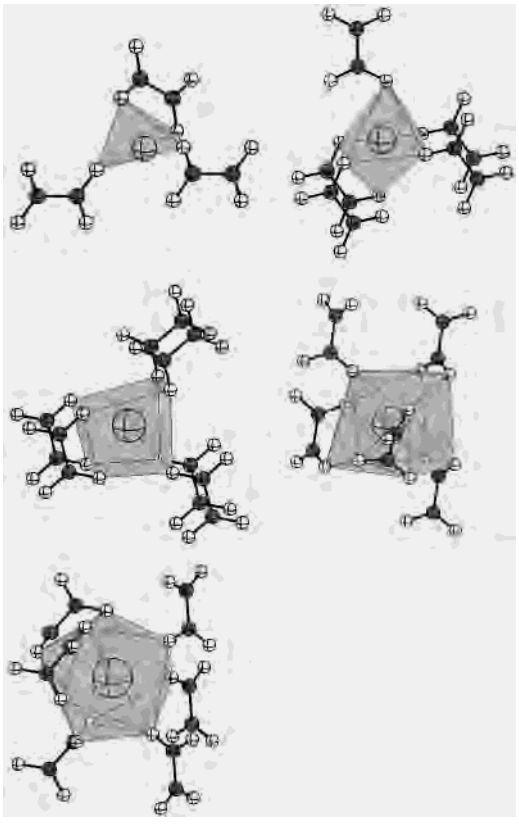

Figure 7. Coordination polyhedra of crystal structures of $A_2C_2O_4$ [A = Li (top left),[16] Na (top right),[17] K, β-Rb (middle left), α-Rb, Cs (A(2) middle right, and A(1) bottom left)]. Oxygen positions are in white, carbon positions are in dark gray, and alkali metal positions and their corresponding polyhedra are in light gray.

cations at $00^1/_2$, $^1/_3{}^2/_30$, and $^2/_3{}^1/_3{}^1/_4$. This is the type of packing found in $Hg_{99}As$ ($P\bar{6}m2$)[39,40] or, alternatively, corresponds to a modification of boron nitride[41] with a vacancy at $^2/_3{}^1/_3{}^1/_4$ (Figure 5).

The oxalate anion itself is twisted by 99(1)° for **III** (94-(3)° for **II**-α) (Figure 3). This can be attributed to packing effects in the cesium (rubidium) compound. The influence of hydrogen bonding as found for other, slightly twisted oxalates can be excluded. The lengthening of the C−C bond of the oxalate anion (>1.54 pm) is consistent for all oxalates and can be explained by MO theory.[42,43]

The crystallographic relationship between these two different crystal structures (*Pbam* and $P2_1/c$) can be understood from the following group−subgroup relationship: *Pbam* → *Pbam* (doubled *c*-axis, which is not observed) → $P2_1/c$. The transformation matrix is given by

$$(a\ \ b\ \ c)_{P2_1/c} = \begin{pmatrix} 0 & 0 & 2 \\ 1 & 0 & 0 \\ 0 & 1 & 0 \end{pmatrix} * (a\ \ b\ \ c)^{T}_{Pbam}$$

Figure 5 shows the relations of the packings of the two different crystal structures in two projections. It is clearly visible that (apart from an internal twist within the oxalate anion) displacive movements of both the alkali cations and the center of gravity locations of the oxalate anions occur.

(39) Puselj, M.; Ban, Z. *J. Less-Common Met.* **1974**, *37*, 213-216.
(40) Donohue, J. *J. Less-Common Met.* **1978**, *57*, 229.
(41) Pease, R. S. *Acta Crystallogr.* **1952**, *5*, 356−361.
(42) Brown, R. D.; Harcourt, R. D. *Aust. J. Chem.* **1963**, *16*, 737−758.
(43) Zhou, G.; Li, W.-K. *J. Chem. Educ.* **1989**, *66*, 572.

No major rearrangements within the crystal structures are necessary.

It may be speculated that the driving force for the structural phase transition between **II**-β and **II**-α is related to the increased polarizability and/or size of the rubidium cation compared to the potassium cation. An unfavorable cation to anion size ratio for a given packing creates stress in certain directions in a crystal structure. This is directly related, via the elastic constants, to the anisotropic microstrain (Figure 2). The latter can be derived from high-resolution powder diffraction data. Three-dimensional anisotropic strain distributions of **I** and **II**-β on an equal scale immediately reveal an increase in strain within the alkali and oxalate layers, respectively, with an increase in the size of the cation. In both cases, the strain perpendicular to the layers is relatively low, leaving the packing in the perpendicular direction essentially unchanged (Figure 5). It should be noted that, for cesium oxalate, no significant anisotropy of the microstrain was found.

The neutral, solvent-free alkali oxalates clearly show a strong dependence of the coordination numbers on the size of the alkali cations, starting with four (tetrahedron, lithium) and increasing to six (octahedron, sodium), eight (cubic, potassium and β-rubidium), and nine and ten (cesium and α-rubidium) (Figure 7). The structure of lithium oxalate[14] consists of planes of corner-shared tetrahedra of LiO_4 connected by planes of oxalate anions (Figure 6). The structure of sodium oxalate[15] is, except for different coordination numbers, similar to those of potassium and β-rubidium oxalate. All consist of a herringbone arrangement of infinite double chains of the corresponding alkali cations interconnected by infinite chains of oxalate anions with a smaller inclination for sodium oxalate (Figure 6). Edge-shared slightly distorted octahedra of NaO_6 form the infinite double chains of sodium which are connected to neighboring double chains via a common corner as in rutile type structures. The structures of the water-containing alkali oxalates are completely different from their corresponding anhydrous compounds.[9,33−37,44]

The band assignments for the vibrational spectra, and the conclusions one can draw from these about the geometry of oxalate anions in solid-state and aqueous solution are still subject to controversial discussions.[45−50] On the basis of the spectra of isotopically pure samples of $K_2{}^{12}C_2O_4{\cdot}H_2O$ and $K_2{}^{13}C_2O_4{\cdot}H_2O$ and the data of $^{14}N_2O_4$ and $^{15}N_2O_4$ as well as corresponding force field studies, it has been recently shown[51,46] that the wavenumbers of the oxalate vibrations, especially the ν(CC) mode, strongly depend on the dihedral angle. The corresponding normal coordinates are represented by a substantial mix of the symmetry coordinates[51] already present in the highest possible symmetry case of D_{2h}. Due to this coupling the lowest and second lowest bands of the totally symmetric modes were reassigned, viz., $\nu_{CC} = 490$ cm^{-1} and $\delta_{CO2} = 894$ cm^{-1}. This reassignment brings the band assignment of $C_2O_4{}^{2-}$ and the isoelectronic and isostructural N_2O_4 in agreement. Therefore, the band assignments of $A_2C_2O_4$ (A = K, Cs), shown in Table 4, are based on these new data.

Table 4. Band Assignment for $A_2C_2O_4$ (A = K, Cs)

K		Cs		assignment (irrep in D_{2h}[51])
IR	Raman	IR	Raman	
	1743			$2\delta_s(CO_2)$
1663 1621		1567 1549		$\nu_{as}(CO_2)$ (b_{2u})
	1649 1619		1557 1538	$\nu_{as}(CO_2)$ (b_{3g})
1561				impurity
	1437	1507 1489	1489	$\nu_s(CO_2)$ (a_{1g})
1325 1309	1324 (vw)	1299	1301 1298	$\nu_{as}(CO_2)$ (b_{1u})
	872		898	$\delta_s(CO_2)$ (a_{1g})
496		855 817	860 822	$\delta_\omega(CO_2)$ (b_{3u})
774 766		741	747 745	$\delta_{as}(CO_2)$ (b_{1u})
			519	$\delta_\omega(CO_2)$ (b_{2g}) (?)
	462		431	ν(CC) (a_{1g}) (?)
	407		300 289	$\delta_\rho(CO_2)$ (b_{2u}/b_{3g})

In the crystal structure of $K_2C_2O_4$ (*oP*16, *Pbam*, dihedral angle = 0°), the oxalate anion is placed on the special site 2*c* of site symmetry C_{2h}. Therefore, 12 and 10 internal modes of the oxalate anion are expected in the Raman and IR spectra, respectively (see correlation table, Table 5). In contrast, the oxalate anion of $Cs_2C_2O_4$ (*mP*32, $P2_1/c$, dihedral angle = 99°) is placed on general sites. All modes of maximum point group symmetry D_2 mix to irreducible representation A for C_1 point group symmetry. Thus, 24 internal modes are expected in the Raman as well as the IR spectra of this compound (see Table 5).

In particular, the rule of mutual exclusion holds for $K_2C_2O_4$ but not for $Cs_2C_2O_4$. As a consequence, the Raman and IR spectra of $K_2C_2O_4$ are complementary, e.g., the Raman spectra exhibit exclusively bands due to gerade modes, while the IR spectra exhibit the ungerade modes (Table 4 and Figure 8). The observed wavenumbers fit quite well to literature values[51] for the planar oxalate anion of D_{2h} symmetry. Except for one band at 1561 cm^{-1}, which is due to a small quantity of an impurity, all bands were assigned to the given fundamentals. Weak bands in the 4000−2000 cm^{-1} region were assigned fully to combination bands and overtones, respectively.

In contrast, the spectra of $Cs_2C_2O_4$ exhibit the $\nu_s(CO_2)$, $\delta_s(CO_2)$, and $\delta_{as}(CO_2)$ modes in either case, due to the

(44) Pedersen, B. F. *Acta Chem. Scand.* **1965**, *19*, 1815−1818.
(45) Ito, K.; Bernstein, H. J. *Can. J. Chem.* **1956**, *34*, 170−178.
(46) Begun, G. M.; Fletcher, W. H. *Spectrochim. Acta* **1963**, *19*, 1343−1349.
(47) Pedersen, B. F. *Acta Chem. Scand.* **1967**, *21*, 801−811.
(48) Shippey, T. A. *J. Mol. Struct.* **1980**, *65*, 61−70.
(49) Shippey, T. A. *J. Mol. Struct.* **1980**, *67*, 223−233.
(50) Hind, A. R.; Bhargava, S. K.; Van Bronswijk, W.; Grocott, S. C.; Eyer, S. L. *Appl. Spectrosc.* **1998**, *52*, 683−691.
(51) Clark, R. J. H.; Firth, S. *Spectrochim. Acta, Part A* **2002**, *58*, 1731−1746.
(52) Hill, R. J.; Cranswick, L. M. D. *J. Appl. Crystallogr.* **1994**, *27*, 802−844.

Table 5. Correlation Table for the Vibrational Modes of $K_2C_2O_4$ and $Cs_2C_2O_4$

	free ion		solid state			
A			site symmetry	space group	activity	
Cs	D_{2d}	D_2	C_1	C_{2h}^5	R	IR
	A_1 (3)	A (4)	A (12)			
	B_1 (1)			A_g (12)	12	
	A_2 (0)	B_1 (2)		A_u (12)		12
	B_2 (2)			B_g (12)	12	
	E (3)	B_2 (3)		B_u (12)		12
		B_3 (3)				
					Σ 24	Σ 24
K	D_{2h}		C_{2h}	D_{2h}^9	R	IR
	A_g (3)		A_g (5)	A_g (5)	5	
	B_{3g} (2)			B_{1g} (5)	5	
	A_u (1)		A_u (2)	A_u (2)		
	B_{3u} (1)			B_{1u} (2)		2
	B_{1g} (0)		B_g (1)	B_{2g} (1)	1	
	B_{2g} (1)			B_{3g} (1)	1	
	B_{1u} (2)		B_u (4)	B_{2u} (4)		4
	B_{2u} (2)			B_{3u} (4)		4
					Σ 12	Σ 10

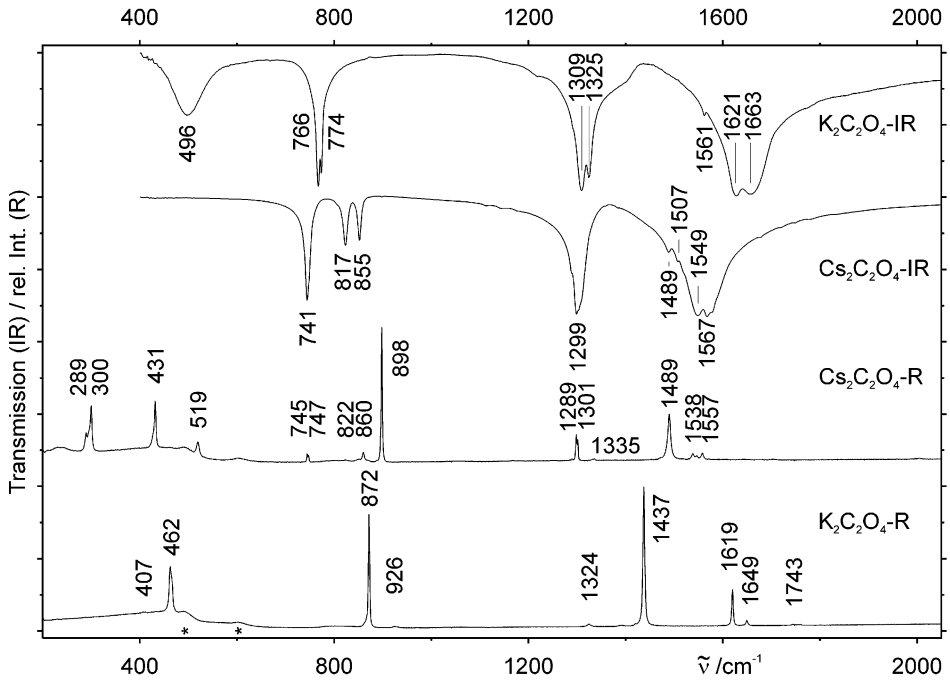

Figure 8. Vibrational spectra of $A_2C_2O_4$ (A = K, Cs; IR, transmission, Raman (R), rel. intensities; all spectra are shifted for clarity, and marked bands correspond to quartz, used as tube material).

breakdown of the law of mutual exclusion in this particular case. Nevertheless, bands assigned to gerade modes in $K_2C_2O_4$ are more intense in the Raman spectra, while those corresponding to ungerade modes in $K_2C_2O_4$ exhibit higher intensities in the IR spectra. Band assignments agreed well with those found for the twisted oxalate anion in ammonium oxalate hydrate.[51] As a consequence of the twist geometry, the ν(CC) and $\delta_\rho(CO_2)$ modes are shifted toward lower wavenumbers in comparison to $K_2C_2O_4$ (Table 4 and Figure 8). Additional strong bands at 855 and 817 cm^{-1} are observed in the IR spectra, which are also observed as very weak bands in the corresponding Raman spectra. Taking into account (i) the high intensities of those bands in the IR spectra, (ii) the reassignments stated above, and (iii) the strong increase

of the $\rho_\omega(CO_2)$ mode on increase of the dihedral angle (526 and 641 cm^{-1} for $\tau = 0°$ and 28°, respectively),[51] those bands very likely arise from the wagging mode $\rho_\omega(CO_2)$, which is observed in the IR spectra of $K_2C_2O_4$ at 496 cm^{-1}.

As a result, the vibrational spectra of $K_2C_2O_4$ and $Cs_2C_2O_4$ are in good agreement with the structures of the oxalate anions derived from the diffraction studies. Due to the phase behavior, the vibrational spectra of as-prepared samples of $Rb_2C_2O_4$ show the prominent bands of the **II**-β as well as the **II**-α modification. Due to this, vibrational spectra of spectroscopically pure samples could not be achieved.

The crystal structures of the higher homologues of the alkali oxalates could be determined from high-resolution X-ray powder diffraction data. More generally speaking, it is now possible, on a fairly routine basis, to solve small molecule structures by high-resolution powder diffraction, within the accuracy of single-crystal diffraction in the early 1960s. This allows us to discuss individual bond lengths and angles. As a result, it has become obvious that the conformation of the oxalate anion, when acting as a weak interacting ligand, is mainly determined by packing effects: bonded to nonpolarizing cations K^+, Rb^+, and Cs^+, the planar as well as the much rarer staggered conformations have been observed.

Acknowledgment. This work was carried out in part at the National Synchrotron Light Source at Brookhaven National Laboratory, which is supported by the US Department of Energy, Division of Materials Sciences and Division of Chemical Sciences. The SUNY X3 beamline at NSLS is supported by the Division of Basic Energy Sciences of the US Department of Energy under Grant No. DE-FG02-86ER45231. Special thanks go to Sanela Kevric (MPI-FKF at Stuttgart) for her support in sample preparation and to Peter Stephens (SUNY at Stony Brook) for his help during data collection. Thanks also go to Marie-Luise Schreiber, Wolfgang König, and Hans Vogt for measuring the IR and Raman data, and to Klaus Hertel (all MPI-FKF at Stuttgart) for the Guinier−Simon measurement. Financial support by the Deutsche Forschungsgemeinschaft (DFG), the Bundesministerium für Bildung und Forschung (BMBF), and the Fonds der Chemischen Industrie (FCI) is gratefully acknowledged.

Supporting Information Available: Crystallographic data (CIF). This material is available free of charge via the Internet at http://pubs.acs.org. CCDC 192180−192183 also contain the supplementary crystallographic data for this paper. These data can be obtained free of charge via www.ccdc.cam.ac.uk/conts/retrieving-.html (or from the CCDC, 12 Union Road, Cambridge CB2 1EZ, U.K.; fax, +44 1223 336033; e-mail, deposit@ccdc.cam.ac.uk).

IC0205536